Available online at www.sciencedirect.com
SCIENCE DIRECT®
International Journal of Solids and Structures 41 (2004) 6335–6350
INTERNATIONAL JOURNAL OF SOLIDS and STRUCTURES
www.elsevier.com/locate/ijsolstr

Elastodynamic Green's functions for a laminated piezoelectric cylinder

H. Bai [a], E. Taciroglu [b], S.B. Dong [b,*], A.H. Shah [c]

[a] *Lakehead University, Thunder Bay, ON, Canada*
[b] *Department of Civil and Environmental Engineering, University of California, Los Angeles, P.O. Box 159310, 2066 Engineering I, Los Angeles, CA 90095-1593, USA*
[c] *The University of Manitoba, Winnipeg, Manitoba, Canada*

Received 3 December 2003; received in revised form 6 May 2004
Available online 10 June 2004

Abstract

Elastodynamic Green's functions for a piezoelectric structure represent the electro-mechanical response due to a steady-state point source as either a unit force or a unit charge. Herein, Green's functions for a laminated circular piezoelectric cylinder are constructed by means of the superposition of modal data from the spectral decomposition of the operator of the equations governing its dynamic behavior. These governing equations are based on a semi-analytical finite element formulation where the discretization occurs through the cylinder's thickness. Examples of a homogeneous PZT-4 cylinder and a two-layer cylinder composed of a PZT-4 material at crystal orientations of $\pm 30^\circ$ with the longitudinal axis are presented. Numerical implementation details for these two circular cylinders show the convergence and accuracy of these Green's functions.

Keywords: Elastodynamic Green's functions; Laminated piezoelectric circular cylinder; Modal superposition

1. Introduction

Free vibration analysis of a structure, or alternatively the spectral decomposition of the operator of its governing equation, yields modal data, which can be used to characterize the structural response due to a myriad of forced inputs. Herein, we are concerned with the construction of Green's functions for a laminated circular cylinder based on modal data established by the procedure of Siao et al. (1994). The cylinder under consideration may be composed of any number of uniform thickness piezoelectric layers, where each layer may have its own material properties. The availability of Green's functions will enable methods to be formulated for examining the wave scattering phenomena in such cylinders in the presence of flaws such as

* Corresponding author. Tel.: +1-310-8255353; fax: +1-310-2062222.
E-mail address: dong@seas.ucla.edu (S.B. Dong).

0020-7683/$ - see front matter © 2004 Elsevier Ltd. All rights reserved.
doi:10.1016/j.ijsolstr.2004.05.017

cracks and delaminations. It is hoped that useful ideas for structural health monitoring will emerge from this path of investigation.

The free axisymmetric and flexural vibrations of a circular piezoelectric cylinder whose material belongs to crystal class 6*mm* were first studied by Paul (1962, 1966). Numerical exploration of his frequency equations in the long wave length regime was first attempted by Paul and Raju (1981, 1982) by means of asymptotic analysis. Subsequently, Paul and Venkatesan (1987) provided numerical data for a wide range of wave lengths under various combinations of opened and shorted circuit conditions on the two lateral surfaces of a hollow cylinder. Ding et al. (1997) and Chen et al. (2004) presented analytic solutions for the free vibration of piezoelectric cylinders filled with a compressible fluid, wherein results for a cylinder without fluid were also given. Buchanan and Peddieson (1989, 1991) computed the natural frequencies of propagating waves for infinitely long piezoelectric cylinders using a one-dimensional finite element model in the radial direction. Siao et al. (1994), employing the same radial discretization procedure and a semi-analytical finite element formulation, determined spectral data for both propagating waves and edge vibrations in such cylinders. More recently, Hussein and Heyliger (1998) presented a free vibration analysis of laminated piezoelectric cylindrical shells using a semi-analytical discrete-layer model. While the bulk of the literature is concerned with free vibration analyses, some studies on forced response have appeared; see, for example, Ding et al. (2003), who considered the transient axisymmetric plane strain response of a hollow piezoelectric cylinder. For additional references on topics related to piezoelectric structures, see Dökmeci (1980, 1989) whose surveys elaborate on a wide range of subjects, including many on finite element calculations.

Siao et al. (1994) presented a method for determining the eigendata for a circular laminated piezoelectric cylinder. Such data consist of a finite basis of propagating waves and edge vibrations, as contrasted with an infinity of these eigenmodes had an analytical solution procedure been used. Nevertheless, such numerical eigendata can be made as accurate as necessary by appropriate discretization of the thickness profile. Since one-dimensional elements are used, the computational cost associated with a very fine model is modest vis-a-vis models based on multi-dimensional interpolations. Herein, we utilize this method to establish the eigendata for construction of an elastodynamic steady-state Green function for such a cylinder. This construction is based on a modal representation of a singular source term. Examples of such Green's functions for two-dimensional laminated anisotropic plates and laminated anisotropic circular cylinders were given by Zhu et al. (1995) and Zhuang et al. (1999), respectively. Green's function is essential to quantitative non-destructive evaluations of crack sizes and locations, delaminations, and other flaws in a structure. They are used to describe the loading conditions on the flaws and they comprise the kernels in boundary element analyses. This approach is attractive because of the relative ease in forming boundary integral in the presence of crack-tip singularity; see, for example, Zhu et al. (1995).

In the next section, the dependent variables are summarized and a non-dimensionalization is invoked. Then, the governing equations of motion and boundary conditions are given and two eigenproblems are discussed. Next, a steady-state solution for a time harmonic forced input is given by means of a Fourier transform. Based on this solution, an elastodynamic Green's function for the laminated piezoelectric cylinder can be constructed. Examples of Green's functions are given for a homogeneous PZT-4 cylinder and for a two-layer cylinder of same material but with their crystallographic axes oriented at $\pm 30^\circ$ with the generator.

2. Preliminaries

Consider an infinitely long laminated piezoelectric circular cylinder as shown in Fig. 1 where cylindrical coordinates (r, θ, z) have been adopted. The primary dependent variables in this problem are: mechanical displacement $\mathbf{u} = [u_r, u_\theta, u_z]^{\mathrm{T}}$; stress $\mathbf{T} = [T_{rr}, T_{\theta\theta}, T_{zz}, T_{\theta z}, T_{rz}, T_{r\theta}]^{\mathrm{T}}$; strain $\mathbf{S} = [S_{rr}, S_{\theta\theta}, S_{zz}, S_{\theta z}, S_{zr}, S_{r\theta}]^{\mathrm{T}}$; electric

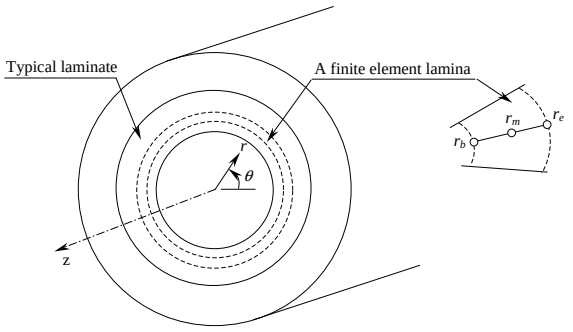

Fig. 1. Laminated piezoelectric cylinder.

displacement $\mathbf{D} = [D_r, D_\theta, D_z]^{\mathrm{T}}$; and electric field $\mathbf{E} = [E_r, E_\theta, E_z]^{\mathrm{T}}$, where $\mathbf{E} = -\nabla\phi$ with ϕ as the electric potential. It is convenient to concatenate the mechanical and electrical dependent variables into arrays.

$$\mathbf{q} = \left\{ \begin{array}{c} \mathbf{S} \\ \mathbf{E} \end{array} \right\}_{9\times 1}, \quad \mathbf{Q} = \left\{ \begin{array}{c} \mathbf{T} \\ \mathbf{D} \end{array} \right\}_{9\times 1}, \quad \mathbf{v} = \left\{ \begin{array}{c} \mathbf{u} \\ \phi \end{array} \right\}_{4\times 1} \tag{1}$$

For a given cylindrical lamina, the piezoelectric constitutive relation in terms of the concatenated variables is given by

$$\mathbf{Q} = \mathbf{C}^{*}\mathbf{q} \quad \text{where} \quad \mathbf{C}^{*} = \begin{pmatrix} \mathbf{c} & -\mathbf{e}^{\mathbf{T}} \\ \mathbf{e} & \boldsymbol{\varepsilon} \end{pmatrix} \tag{2}$$

with $\mathbf{c}$, $\mathbf{e}$ and $\boldsymbol{\varepsilon}$ as the matrices of the elastic anisotropic moduli (6×6), piezoelectric constants (3×6) and dielectric constants (3×3), respectively. Also, there are nine generalized deformational relations, $\mathbf{q} = \mathbf{L}\mathbf{v}$, where operator $\mathbf{L}$ contains the linear cylindrical coordinates differential operators relating the strain and electric field to the mechanical displacement and potential.

Dimensionless variables are used herein to preclude numerical anomalies due to large differences in the units between the various material properties. In setting forth this non-dimensionalization, regard all quantities on the right-hand and left-hand sides, respectively, of each defining equation to be the dimensional and their corresponding dimensionless form. Four key properties are selected as the reference values, viz., (1) total cylinder thickness h, (2) an elastic modulus, c^0, (3) a piezoelectric constant e^0, and (4) mass density ρ^0 where c^0, e^0 and ρ^0 are of a particular laminate in the cylinder's radial profile. The geometry and mechanical displacements, the material constants and mass densities are normalized as

$$r = \frac{r}{h}, \quad z = \frac{z}{h}, \quad u_i = \frac{u_i}{h}, \quad (i = r, \theta, z) \tag{3}$$

$$c_{pq} = \frac{c_{pq}}{c^0}, \quad \varepsilon_{ij} = \frac{\varepsilon_{ij}}{\varepsilon^0}, \quad e_{ip} = \frac{e_{ip}}{e^0}, \quad \rho_i = \frac{\rho_i}{\rho^0}, \qquad (p, q = 1, 2, 3, \ldots, 6); \quad (i, j = 1, 2, 3) \tag{4}$$

where ε^0 is the reference dielectric constant given by $\varepsilon^0 = (e^0)^2/c^0$. Introduce E^0 and t^0 as

$$E^0 = \frac{c^0}{e^0}, \quad t^0 = \sqrt{\frac{\rho^0}{c^0}}h \tag{5}$$

With these parameters, time t and electric potential ϕ take the non-dimensional forms

$$t = \frac{t}{t^0} \quad \text{and} \quad \phi = \frac{\phi}{E^0 h} \tag{6}$$

All of the other variables are rendered dimensionless by

$$T_p = \frac{T_p}{c^0}, \quad S_p = S_p, \ (p = 1, 2, \ldots, 6); \qquad D_k = \frac{D_k}{e^0}, \quad E_k = \frac{E_k}{E^0}, \ (k = 1, 2, 3) \tag{7}$$

Lastly, the normalized charge ρ_e and body force density component f_i are given by

$$\rho_e = \frac{h\rho_e}{e^0}, \quad f_i = \frac{hf_i}{c^0}, \ (i = r, \theta, z) \tag{8}$$

This non-dimensionalization scheme yields all dimensionless equations in the same form as their dimensional counterparts.

3. Governing equation and boundary conditions

The equations of motion in Siao et al. (1994) are based on a semi-analytical finite element formulation, where the discretization of the laminated cylinder takes the form of a series of three-node cylindrical laminas, each capable of having its own piezoelectric properties and thickness. In each three-node element, a quadratic interpolation field is used radially but the axial, circumferential and time dependencies are left undetermined at the outset. Hamilton's principle with Tiersten's (1969) electric enthalpy as the energy functional was used to derive the following matrix equations of motion.

$$\mathbf{K}_1\mathbf{V} + \mathbf{K}_2\mathbf{V}_{,\theta} + \mathbf{K}_3\mathbf{V}_{,\mathbf{z}} - \mathbf{K}_4\mathbf{V}_{,\theta\theta} - \mathbf{K}_5\mathbf{V}_{,\theta z} - \mathbf{K}_6\mathbf{V}_{,\mathbf{zz}} + \mathbf{M}\ddot{\mathbf{V}} = \mathbf{F} \tag{9}$$

where $\mathbf{V}$ is an ordered set of nodal variables for all of the nodes in the finite element model of the cylinder. The stiffness and consistent mass matrices, $\mathbf{K}_i$'s and, $\mathbf{M}$ can be found in Siao et al. (1994), where $\mathbf{K}_1$, $\mathbf{K}_4$, $\mathbf{K}_5$ and $\mathbf{K}_6$ are symmetric, while $\mathbf{K}_2$ and $\mathbf{K}_3$ are antisymmetric. The consistent load $\mathbf{F}$ is obtained by integrating the product of the radial interpolation functions $\mathbf{N}$ and the mechanical loads and electric charge over the radial profile of the cylinder.

$$\mathbf{F} = \int_r \mathbf{N}^{\mathrm{T}} \begin{bmatrix} \mathbf{f} \\ -\rho_e \end{bmatrix} r \, \mathrm{d}r \tag{10}$$

where $\mathbf{f}$ contains the components of the mechanical load and ρ_e is the charge density.

Homogeneous boundary conditions on the lateral surfaces and end cross-section can be stated as follows. For a hollow cylinder with inside and outside radii, r_{in} and r_{out}, traction-free surfaces require that

$$T_{rr} = T_{r\theta} = T_{zr} = 0 \tag{11}$$

The electrical condition may take the form of an opened circuit (surface is uncoated) where the radial electric displacement component D_r must vanish or a shorted-circuited condition (a coated lateral surface that is grounded) where the potential ϕ (or voltage) vanishes

$$D_r = 0 \quad \text{or} \quad \phi = 0 \tag{12}$$

4. Free vibration analyses

For free vibrations, the solution form is

$$\mathbf{V} = \mathbf{V}_m \exp\{\mathrm{i}(k_m z + m\theta - \omega t)\} \tag{13}$$

where ω is the circular frequency, (k_m, m) are the axial and circumferential wave numbers, and $\mathbf{V}_m$ is the array of nodal coordinates in the radial profile of the finite element discretization. Substitution of solution form (13) into the homogeneous form of Eq. (9) gives

$$(\mathbf{K}_1 + \mathrm{i}m\mathbf{K}_2 + \mathrm{i}k_m\mathbf{K}_3 + m^2\mathbf{K}_4 + mk_m\mathbf{K}_5 + k_m^2\mathbf{K}_6)\mathbf{V}_m - \omega^2\mathbf{M}\mathbf{V}_m = 0 \tag{14}$$

For circumferential periodicity, integer values must be used for circumferential mode number m. Two eigenproblems can be deduced depending on whether ω^2 or k_m is chosen as the eigenvalue.

If ω^2 is taken as the eigenvalue, then wave number k_m assumes assigned values in Eq. (14). This system is Hermitian, since the real and purely imaginary matrices are symmetric and antisymmetric, respectively, and only real eigenvalues ω^2 are admitted. Doubling the algebraic eigensystem size reveals its real, symmetric positive-definiteness.

$$\begin{pmatrix} \mathbf{K}_1 + m^2\mathbf{K}_4 + k_m m\mathbf{K}_5 + k_m^2\mathbf{K}_6 & -(m\mathbf{K}_2 + k_m\mathbf{K}_3) \\ (m\mathbf{K}_2 + k_m\mathbf{K}_3) & \mathbf{K}_1 + m^2\mathbf{K}_4 + k_m m\mathbf{K}_5 + k_m^2\mathbf{K}_6 \end{pmatrix} \begin{pmatrix} \mathbf{V}_m \\ -\mathbf{V}_m \end{pmatrix} = \omega^2 \begin{pmatrix} \mathbf{M} & 0 \\ 0 & \mathbf{M} \end{pmatrix} \begin{pmatrix} \mathbf{V}_m \\ -\mathbf{V}_m \end{pmatrix} \tag{15}$$

This eigenproblem consists of two identical subsystems, so that the eigensolution yields pairs of real ω^2 representing the same wave form except with a phase difference of $\pi/2$. This eigenproblem, denoted as EVP1, is useful for establishing the frequency spectra for propagating modes.

If k_m serves as the eigenvalue with assigned values for ω^2, Eq. (14) takes the form of a second order algebraic eigenproblem.

$$(\mathbf{K}_1 + m^2\mathbf{K}_4 - \omega^2 M + \mathrm{i}m\mathbf{K}_2)\mathbf{V}_m + k_m(m\mathbf{K}_5 + \mathrm{i}\mathbf{K}_3)\mathbf{V}_m + k_m^2\mathbf{K}_6\mathbf{V}_m = 0 \tag{16}$$

This eigenproblem, denoted as EVP2, can be converted to the following first order form

$$\left(\begin{bmatrix} 0 & \mathbf{I} \\ -(\mathbf{K}_1 + m^2\mathbf{K}_4 - \omega^2\mathbf{M} + \mathrm{i}m\mathbf{K}_2) & -(m\mathbf{K}_5 + \mathrm{i}\mathbf{K}_3) \end{bmatrix} - k_m \begin{bmatrix} \mathbf{I} & \\ & \mathbf{K}_6 \end{bmatrix} \right) \begin{pmatrix} \mathbf{V}_m \\ k_m\mathbf{V}_m \end{pmatrix} = 0 \tag{17a}$$

or in abbreviated form as

$$[\mathbf{A} - k_m\mathbf{B}]\overline{\mathbf{V}}_\mathbf{m} = \mathbf{0} \tag{17b}$$

For a non-trivial solution of Eq. (17a), the determinant must vanish.

$$\det[\mathbf{A} - k_m\mathbf{B}] = 0 \tag{18}$$

Expansion of this determinant yields a polynomial equation for the eigenvalues. This equation serves as the dispersion relation for our piezoelectric finite element model. If $\mathbf{V}_m$ is of dimension N, then system (17a) is $2N$, and there will be $2N$ roots. Denote these roots by $k_{mn} = k_{mn}(m, \omega^2)$; they represent axial wave numbers and can be real or complex-conjugate pairs. A real wave number k_{mn} is associated with a propagating wave, and a purely imaginary or complex conjugate pair k_{mn} portrays a standing vibration in a semi-infinitely long cylinder in which the amplitude exhibits monotonic or sinusoidal decay away from the origin. Associated with each k_{mn} are right and left eigenvectors, $\boldsymbol{\varphi}_{mn}$ and $\boldsymbol{\Psi}_{mn}$ representing the thickness distributions of the nodal displacement and electric potential. They satisfy the equations

$$[\mathbf{A} - k_{mn}\mathbf{B}]\boldsymbol{\varphi}_{mn} = 0 \quad \text{and} \quad \left[\mathbf{A}^{\mathrm{T}} - k_{mn}\mathbf{B}\right]\boldsymbol{\Psi}_{mn} = 0 \tag{19}$$

The eigendata can be divided into two groups, one for traveling or decaying modes from the origin in the positive z-direction and the other for motions in the opposite direction.

Furthermore, the right and left eigenvectors also satisfy the bi-orthogonality relations

$$\boldsymbol{\Psi}_{mq}^{\mathrm{T}}\mathbf{B}\boldsymbol{\varphi}_{mp} = \delta_{pq}B_{mp}, \quad \boldsymbol{\Psi}_{mq}^{\mathrm{T}}\mathbf{A}\boldsymbol{\varphi}_{mp} = \delta_{pq}k_{mp}B_{mp}, \quad (p, q = 1, 2, \ldots, 2N) \tag{20}$$

where δ_{pq} is the Kronecker delta. The eigenvectors can also be partitioned into upper and lower halves as

$$\boldsymbol{\varphi}_{mp} = \begin{Bmatrix} \boldsymbol{\phi}_{mpu} \\ \boldsymbol{\varphi}_{mpl} \end{Bmatrix} = \quad \boldsymbol{\Psi}_{mp} = \begin{Bmatrix} \boldsymbol{\Psi}_{mpu} \\ \boldsymbol{\Psi}_{mpl} \end{Bmatrix} \begin{Bmatrix} \boldsymbol{\varphi}_{mpu} \\ k_{mp}\boldsymbol{\varphi}_{mpu} \end{Bmatrix} \tag{21}$$

In view of this partitioning, the orthogonality relations are

$$\begin{aligned} &\boldsymbol{\Psi}^{\mathrm{T}}_{mqu}\boldsymbol{\varphi}_{mpu} + k_{mp}\boldsymbol{\Psi}^{\mathrm{T}}_{mql}\mathbf{K}_6\boldsymbol{\varphi}_{mpu} = \delta_{pq}B_{mp} \\ &k_{mp}\boldsymbol{\Psi}^{\mathrm{T}}_{mqu}\boldsymbol{\varphi}_{mpu} - \boldsymbol{\Psi}^{\mathrm{T}}_{mql}[\mathbf{K}_1 + m^2\mathbf{K}_4 - \omega^2\mathbf{M} + \mathrm{i}m\mathbf{K}_2]\boldsymbol{\varphi}_{mpu} - k_{mp}\boldsymbol{\Psi}^{\mathrm{T}}_{mql}[m\mathbf{K}_5 + \mathrm{i}\mathbf{K}_3]\boldsymbol{\varphi}_{mpu} = \delta_{pq}k_{mp}B_{mp} \end{aligned} \tag{22}$$

The results by a computer code prepared for this paper were compared with the data of Paul and Venkatesan (1987) as well as from data based on their analytical frequency equation. Also, comparisons were made with that of Siao et al. (1994) using their material data, which should be noted were not normalized by the free permittivity ε_0 factor. Accuracies of three and four significant digits in frequencies and wave numbers were seen.

Spectral plots

Two cylinders are considered herein; both composed of a PZT-4 material, whose properties are given in Berlincourt et al. (1964). One cylinder is homogeneous, with the crystallographic axes oriented with the coordinate directions and the properties are

$$\mathbf{c} = \begin{bmatrix} 5.42969 & 3.03906 & 2.90234 & \cdot & \cdot & \cdot \\ \cdot & 5.42969 & 2.90234 & \cdot & \cdot & \cdot \\ \cdot & \cdot & 4.49219 & \cdot & \cdot & \cdot \\ \cdot & \cdot & \cdot & 1.0 & \cdot & \cdot \\ \cdot & \text{symmetric} & \cdot & \cdot & 1.0 & \cdot \\ \cdot & \cdot & \cdot & \cdot & \cdot & 1.19531 \end{bmatrix}_{0^\circ} \tag{23}$$

$$\mathbf{e} = \begin{bmatrix} \cdot & \cdot & \cdot & \cdot & 0.84106 & \cdot \\ \cdot & \cdot & \cdot & 0.84106 & \cdot & \cdot \\ -0.34437 & -0.34437 & 1.0 & \cdot & \cdot & \cdot \end{bmatrix}_{0^\circ} \tag{24}$$

$$\boldsymbol{\varepsilon} = \begin{bmatrix} 1.46632 & \cdot & \cdot \\ \cdot & 1.46632 & \cdot \\ \cdot & \cdot & 1.29229 \end{bmatrix}_{0^\circ} \tag{25}$$

where the four key reference parameters are (1) $h = 1$ m, (2) $c^0 = c_{44} = 25.6$ GPA, (3) $e^0 = e_{33} = 15.1$ C/m^2 and (4) $\rho^0 = 7.50 \times 10^4$ kg/m^3 so that $\varepsilon^0 = 8.90664 \times 10^{-9}$ F/m and $E^0 = 1.69536 \times 10^9$ N/C. The other cylinder is composed of two-layers. Each layer has thickness $h = 1/2$ m, and the longitudinal crystallographic axes of the two-layers are at $\pm 30^\circ$ with the generator of the cylinder. The properties in this case are

$$\mathbf{c} = \begin{bmatrix} 5.42969 & 3.00488 & 2.93652 & \mp 0.05920 & \cdot & \cdot \\ \cdot & 5.17334 & 2.92432 & \mp 0.21566 & \cdot & \cdot \\ \cdot & \cdot & 4.70459 & \mp 0.19029 & \cdot & \cdot \\ \cdot & \cdot & \cdot & 1.02197 & \cdot & \cdot \\ \cdot & \text{symmetric} & \cdot & \cdot & 1.04883 & \mp 0.08457 \\ \cdot & \cdot & \cdot & \cdot & \cdot & 1.14648 \end{bmatrix}_{\pm 30^\circ} \tag{26}$$

$$\mathbf{e} = \begin{bmatrix} \cdot & \cdot & \cdot & \cdot & 0.72838 & \pm 0.42053 \\ \mp 0.17219 & \pm 0.62666 & \mp 0.29884 & 0.65525 & \cdot & \cdot \\ -0.29823 & -0.37136 & 0.93915 & \pm 0.29387 & \cdot & \cdot \end{bmatrix}_{\pm 30^\circ} \tag{27}$$

$$\varepsilon = \begin{bmatrix} 1.46632 & \cdot & \cdot \\ \cdot & 1.42280 & \mp 0.07535 \\ \text{sym} & \cdot & 1.33581 \end{bmatrix}_{\pm 30^\circ} \tag{28}$$

Based on these values, the normalized frequency is given by

$$\omega = \frac{\omega}{\omega_0} \quad \text{where} \quad \omega_0 = \frac{1}{h}\sqrt{c^0/\rho^0} = 584.24 \text{ rad/s}. \tag{29}$$

Using a finite element model of 30 elements for the homogeneous PZT-4 cylinder, spectral data for circumferential mode numbers $m = 0, 1$ and shorted conditions on the inside and outside lateral surfaces were determined. In Fig. 2, three-dimensional spectral plots for the homogeneous cylinder for circumferential mode numbers $m = 0$ and 1 with shorted circuit lateral surface conditions are shown. In these plots, the real and imaginary wave numbers k_m are normalized by the thickness h, i.e., $\mathrm{Re}(k_m h)$, and $\mathrm{Im}(k_m h)$, and the normalized frequency is shown. A comparison of the frequency spectra of the propagating modes for opened–opened and shorted–shorted lateral surface conditions for $(m = 0, 1)$ is shown in Fig. 3. Observe that there are spectral curves with dips that signify the presence of waves with negative group velocities. This information is useful to have in energy conservation calculations in the study of reflected waves at the free end of a semi-infinitely long cylinder subjected to a monochromatic incident wave. It is seen from Fig. 3 that there is no difference in the torsional spectra for these two cases. A three-dimensional plot of the frequency spectra for the two-layer ±30° angle-ply piezoelectric cylinder with opened–opened lateral surface conditions is shown in Fig. 4. The characteristics in this plot are noticeably different to that for the homogeneous cylinder.

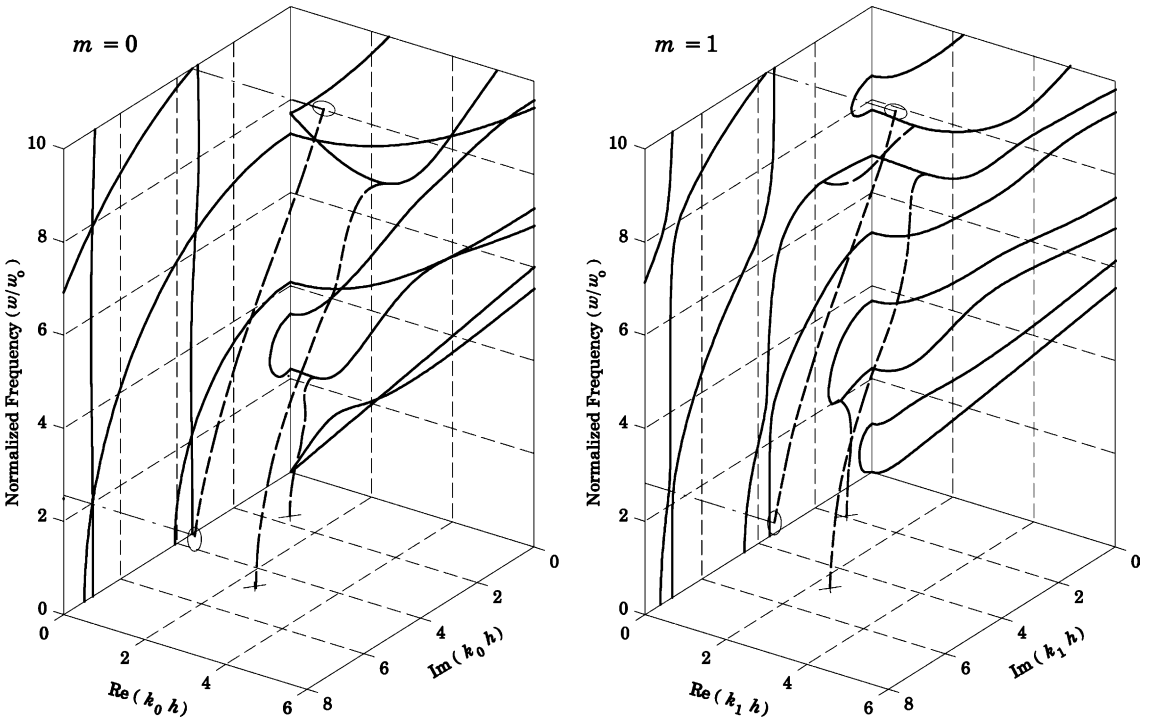

Fig. 2. Three-dimensional spectra for homogeneous piezoelectric cylinder for $m = 0$ and 1, shorted–shorted circuit lateral surface conditions.

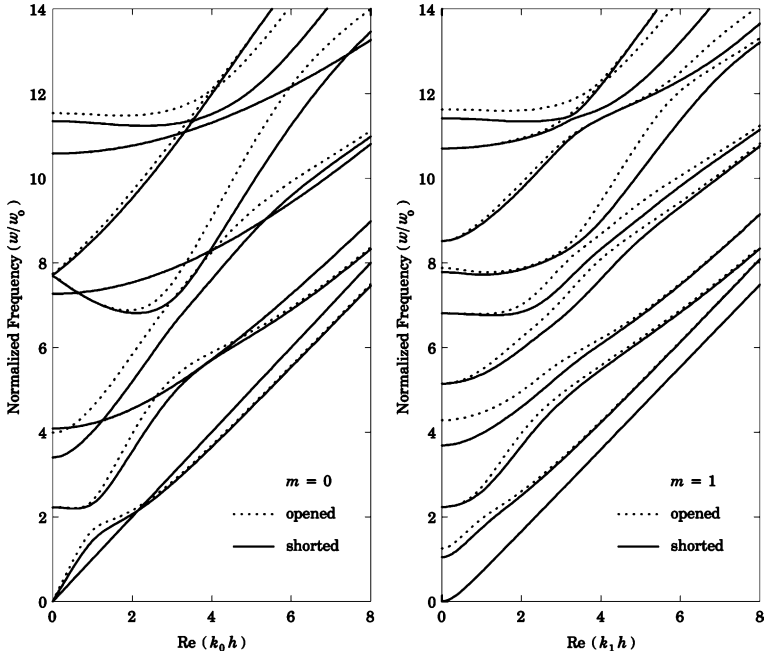

Fig. 3. Frequency spectra comparison between opened–opened and shorted–shorted circuit conditions for $m = 0$ and 1.

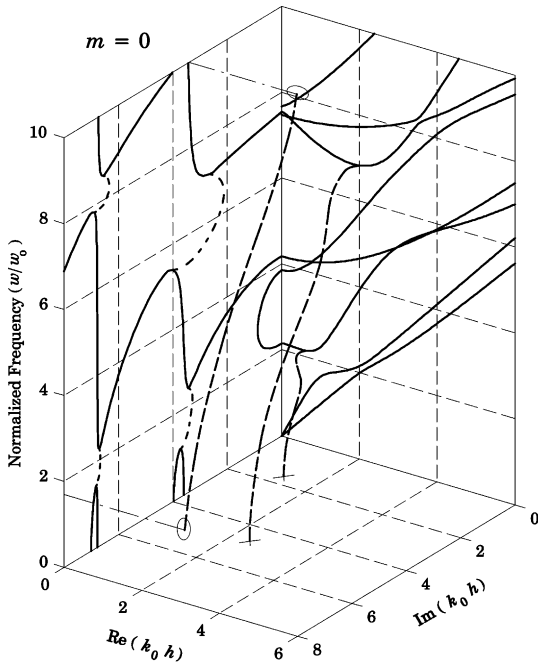

Fig. 4. Three-dimensional spectra for two-layer ±30° piezoelectric cylinder For $m = 0$, opened–opened circuit lateral surface conditions.

5. Forced response to a steady-state load

Let $\mathbf{F}$ in Eq. (9) be a time harmonic load of frequency ω. The θ-dependence of the load and hence the response V can be expressed by Fourier series as

$$\mathbf{F}(\theta,z,t)=\mathrm{e}^{-\mathrm{i}\omega t}\sum_{m=-\infty}^{\infty}\mathbf{F}_m(z)\mathrm{e}^{\mathrm{i}m\theta}\quad\text{and}\quad\mathbf{V}(\theta,z,t)=\mathrm{e}^{-\mathrm{i}\omega t}\sum_{m=-\infty}^{\infty}\mathbf{V}_m(z)\mathrm{e}^{\mathrm{i}m\theta}\tag{30}$$

Substitution of Eq. (30) into (9) and suppressing the common factors give a series of differential equations in m, each of the form

$$\mathbf{K}_6\frac{\mathrm{d}^2\mathbf{V}_m}{\mathrm{d}z^2}+\mathrm{i}[m\mathbf{K}_5+\mathrm{i}\mathbf{K}_3]\frac{\mathrm{d}\mathbf{V}_m}{\mathrm{d}z}-[\mathbf{K}_1+m^2\mathbf{K}_4-\omega^2\mathbf{M}+\mathrm{i}m\mathbf{K}_2]\mathbf{V}_m+\mathbf{F}_m=0\tag{31}$$

where the coefficient matrices of the differential operators are Hermitian.

A Fourier transform is used here to remove the z-dependence, where the Fourier transform pairs are

$$\tilde{\mathbf{v}}_m(k_m)=\int_{-\infty}^{\infty}\mathbf{V}_m(z)\mathrm{e}^{-\mathrm{i}k_mz}\,\mathrm{d}z,\quad\mathbf{V}_m(z)=\frac{1}{2\pi}\int_{-\infty}^{\infty}\tilde{\mathbf{v}}_m(k_m)\mathrm{e}^{\mathrm{i}k_mz}\,\mathrm{d}k_m\tag{32}$$

The Fourier transform to Eq. (31) yields the algebraic equation.

$$\big(k_m^2\mathbf{K}_6+k_m[m\mathbf{K}_5+\mathrm{i}\mathbf{K}_3]+[\mathbf{K}_1+m^2\mathbf{K}_4-\omega^2\mathbf{M}+\mathrm{i}m\mathbf{K}_2]\big)\tilde{\mathbf{v}}_m=\tilde{\mathbf{f}}_m\tag{33}$$

Eq. (33) governs the mth circumferential harmonic in the transformed domain. The first step in the solution of Eq. (33) involves the homogeneous equation, which is in fact EVP2, where the spectral decomposition of the governing operator provides the complete set of eigendata. Thus, the solution of Eq. (33) can be represented by a modal summation of the right eigenvectors, i.e.,

$$\tilde{\mathbf{v}}_m=\sum_{n=1}^{2N}\chi_{mn}\boldsymbol{\varphi}_{mnu}\tag{34}$$

where the coefficients χ_{mn}'s are evaluated by substituting Eq. (34) into Eq. (33) and using bi-orthogonality relations (22). With some algebra, the solution vector $\tilde{\mathbf{v}}_m$ in terms of the upper and lower half eigenvectors can be put into the form

$$\tilde{\mathbf{v}}_m=\sum_{n=1}^{2N}\frac{\boldsymbol{\Psi}_{mnl}^{\mathrm{T}}\tilde{\mathbf{f}}_m}{(k_m-k_{mn})B_{mn}}\boldsymbol{\varphi}_{mnu}\tag{35}$$

The inverse Fourier transform of Eq. (35) recovers the axial dependence of the mth circumferential harmonic.

$$\mathbf{V}_m(z)=\frac{1}{2\pi}\sum_{n=1}^{2N}\int_{-\infty}^{\infty}\frac{\boldsymbol{\Psi}_{mnl}^{\mathrm{T}}\tilde{\mathbf{f}}_m}{(k_m-k_{mn})B_{mn}}\boldsymbol{\varphi}_{mnu}\mathrm{e}^{\mathrm{i}k_mz}\,\mathrm{d}k_m\tag{36}$$

In many problems, $\tilde{\mathbf{f}}_m$, $\boldsymbol{\Psi}_{mn}$, $\boldsymbol{\varphi}_{mn}$ and B_{mn} will be independent of wave number k_m, so that application of the Cauchy residue theorem yields the modal response in a straightforward way. As the eigendata can be divided into two groups, κ_m^+ and κ_m^-, according to traveling and decaying motions from the origin along the positive and negative z-directions, then $\mathbf{V}_m(z)$ can be written as

$$\mathbf{V}_m(z)=\mathrm{i}\sum_{k_{mn}\in\kappa_m^+}\frac{\boldsymbol{\Psi}_{mnl}^{\mathrm{T}}\tilde{\mathbf{f}}_m}{B_{mn}}\boldsymbol{\varphi}_{mnu}\mathrm{e}^{\mathrm{i}k_{mn}z}+\mathrm{i}\sum_{k_{mn}\in\kappa_m^-}\frac{\boldsymbol{\Psi}_{mnl}^{\mathrm{T}}\tilde{\mathbf{f}}_m}{B_{mn}}\boldsymbol{\varphi}_{mnu}\mathrm{e}^{\mathrm{i}k_{mn}z}\tag{37}$$

6. Steady-state Green's function

For construction of Green's function, consider a unit steady-state concentrated force or charge at a source point in the cross-sectional plane $z = 0$ at $\theta = 0$ and some radial distance r_0. For convenience of discussion, let r_0 coincide with a nodal surface. In representing this concentrated source load in Eq. (9), $\mathbf{F}(\theta, z)$ takes the form

$$\mathbf{F}(\theta, z) = \delta(\theta)\delta(z)\mathbf{F}_0 \tag{38}$$

where $\delta(\cdot)$ is the Dirac delta function. The vector $\mathbf{F}_0$ is used to define the location and type of the unit point source, i.e., a unit force or a unit charge. Thus, $\mathbf{F}_0$ will contain zero entries throughout except at nodal surface $r = r_0$ where either a load with components $(\alpha_r, \alpha_\theta, \alpha_z)$ or a unit charge $\alpha_q = 1$ is prescribed.

Since our forced vibration solution procedure involves the expansion of $\delta(\theta)$ in Fourier series and it is well known that such a representation of it does not converge, it is necessary to replace the point source by a uniform spatial pulse of intensity q_0 over a narrow circumferential wide $2r_0\theta_0$ For equivalence of a unit concentrated load, q_0 is given by

$$\int_{-\theta_0}^{\theta_0} q_0 r_0 \, \mathrm{d}\theta = 1 \quad \text{or} \quad q_0 = \frac{1}{2r_0\theta_0} \tag{39}$$

For the case of a unit electric charge, the charge density ρ_e will have the corresponding form

$$\rho_e = \frac{1}{2r_0\theta_0} \tag{40}$$

Therefore, $\mathbf{F}(\theta, z)$ in Eq. (38), for a unit force or unit charge, takes the form

$$\mathbf{F}(\theta, z) = \sum_{m=-\infty}^{\infty} \mathrm{e}^{\mathrm{i}m\theta}\mathbf{F}_m(z) \quad \text{where} \quad \mathbf{F}_m(z) = \frac{1}{2\pi r_0}\frac{\sin m\theta_0}{m\theta_0}\mathbf{F}_0\delta(z) \tag{41}$$

and its Fourier transform is

$$\tilde{\mathbf{f}}_m(k_m) = \frac{1}{2\pi r_0}\frac{\sin m\theta_0}{m\theta_0}\mathbf{F}_0 \tag{42}$$

Substituting of Eq. (42) into Eq. (37) and considering motions only in the positive z-direction yield the mth circumferential mode of displacement Green function. Thus the steady-state unit concentrated generalized force point source takes the form of a series of circular ring-like sources. The displacement Green function is then represented by the summation of these individual circumferential modal responses, i.e.,

$$\mathbf{V}(z) = \sum_{m=-\infty}^{\infty} \mathbf{V}_m(z) = \frac{\mathrm{i}}{2\pi r_0}\sum_{m=-\infty}^{\infty}\frac{\sin m\theta_0}{m\theta_0}\sum_{k_{mn}\in\kappa_m^+}\frac{(\boldsymbol{\Psi}_{mnl})^{\mathrm{T}}\mathbf{F}_0}{B_{mn}}\boldsymbol{\varphi}_{mnu}\mathrm{e}^{\mathrm{i}k_{mn}z}, \quad z \geqslant 0 \tag{43}$$

7. Numerical examples

The precision of Green's function is tied to the number of terms used in the double series representation. Each series entails its own issues, and they were discussed in Zhuang et al. (1999) for a mechanical cylinder. Their conclusions will be seen to apply here equally well from the discussion of our numerical examples.

In the representation of a point load, in the circumferential direction by a uniform pulse over a short arc length, Zhuang et al. (1999) gave a plot showing the number of modes versus pulse width for accuracies from 90% to 99%. This plot serves as guidance for a unit charge since it is merely another point source.

Even though a relatively large number of terms are needed for representing a uniform pulse over a short circumferential distance, Zhuang et al. (1999) demonstrated that substantially fewer terms were required for comparable accuracy of the stresses and displacements. The following examples, using the same two cylinders for which spectral plots were given in Section 4, will show the same convergence rates. In both examples, a normalized steady-state frequency of $\omega = 1.5$ was used.

7.1. Homogeneous PZT-4 cylinder

In this example, both opened–opened and shorted–shorted circuit surface conditions were considered. The unit load requires ring-like circumferential loads to be summed. With regards to this circumferential

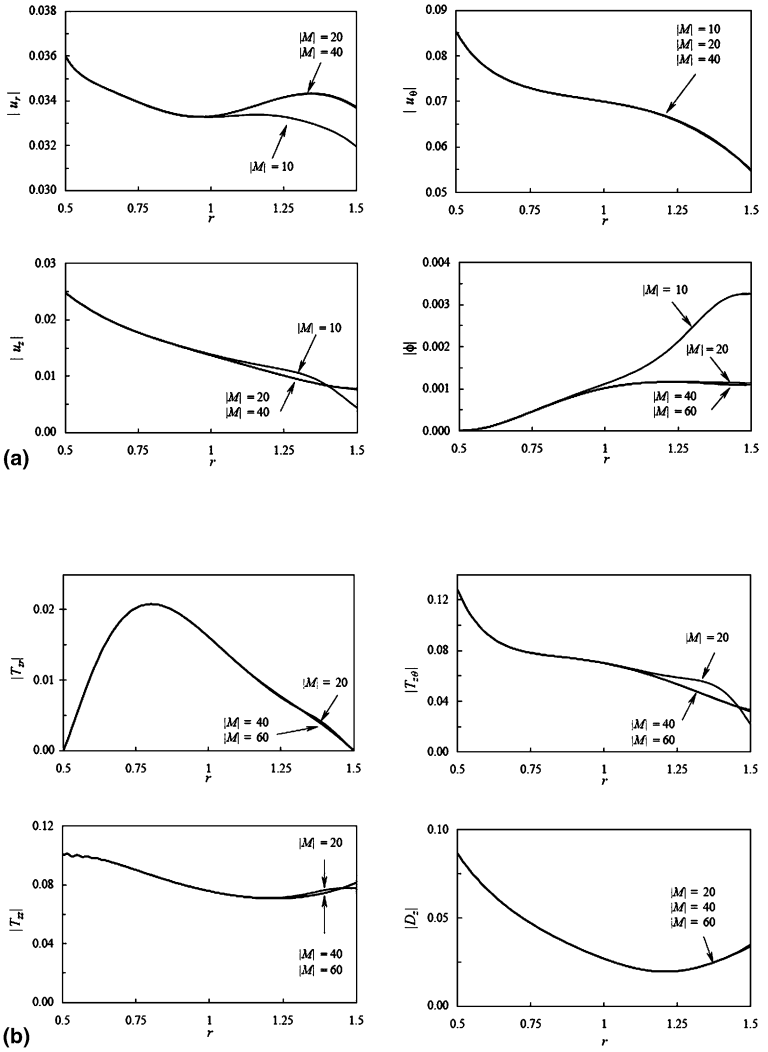

Fig. 5. (a) Comparison of generalized displacements of Green's function for homogeneous PZT-4 cylinder due to unit radial force, opened–opened circuit conditions. (b) Comparison of generalized stresses of Green's function for homogeneous PZT-4 cylinder due to unit radial force, opened–opened circuit conditions.

summation for representation of the force and charge point sources acting on the outer surface of the cylinder, these source terms were approximated by a uniform pulse over a half circumferential width of 0.001 radians. The response was calculated with sum total of circumferential mode numbers of $m = 10$, 20, 40, 60, 80 and 100. As the accuracy is also related to the discretized profile, different size models, i.e., 10, 20, 30, 40, 50 and 60 elements were used. For all circumferential wave numbers, at least 30 elements were observed to be sufficient for good precision of the near-field quantities, which were examined at $\theta = \pi/4$ and $z = h/4$. For the specific case of a unit radial point load on the outer surface, the convergence characteristics as a function of number of circumferential modes are shown in Fig. 5(a and b). With a 30 element model, displacements and potential converged within twenty (20) circumferential modes, and stresses and electric displacement component D_z with forty (40) modes. Sums with more than these minimum numbers

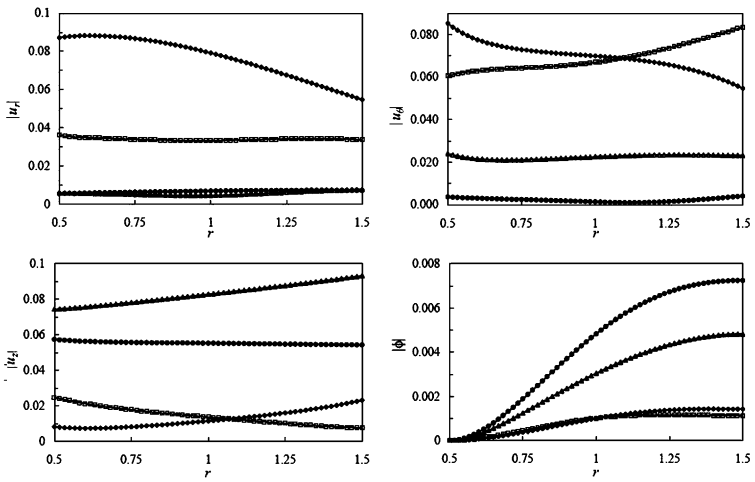

Fig. 6. Generalized displacements in an opened–opened cylinder along $(r, \pi/4, h/4)$ due to external loads applied at $(r_{\text{out}}, 0, 0)$ for $\omega = 1.5$ ((—□—): radial load, (—◇—): circumferential load, (—△—): axial load, (—○—): point charge).

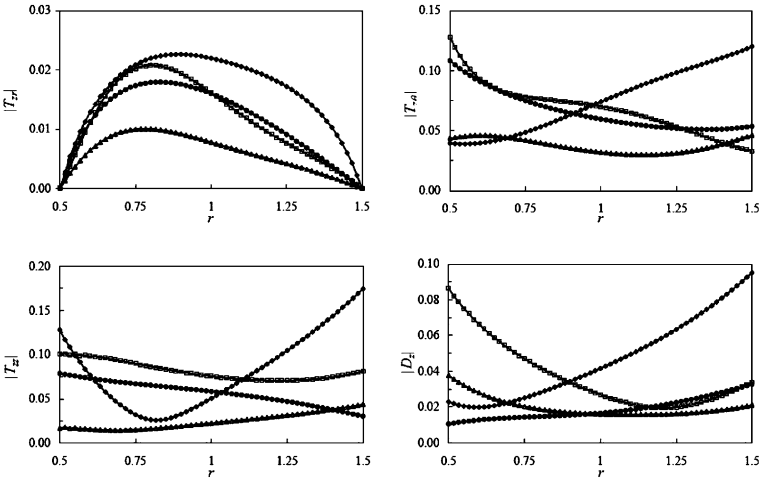

Fig. 7. Generalized stresses in an opened–opened cylinder along $(r, \pi/4, h/4)$ due to external loads applied at $(r_{\text{out}}, 0, 0)$ for $\omega = 1.5$ ((—□—): radial load, (—◇—): circumferential load, (—△—): axial load, (—○—): point charge).

of modes showed a diminishing return on further accuracy. It is not surprising that more terms are needed for stresses than displacements since stress calculations require differentiation of the kinematic field. In examining the balance between the work of the ring-like source and the energy of the response field, differences of less than 0.01% were observed for all the cases.

Displacement, stress, electric displacement and potential profiles at the near field location of $(\theta, z) = (\pi/4, h/4)$ are shown in Figs. 6–9 for opened–opened and shorted–shorted circuit conditions, respectively, and for the complete ser of point sources. Obviously, there are no results for a surface charge in Figs. 8 and 9 since the outer surface is grounded. Also note that since the electric potential is known only

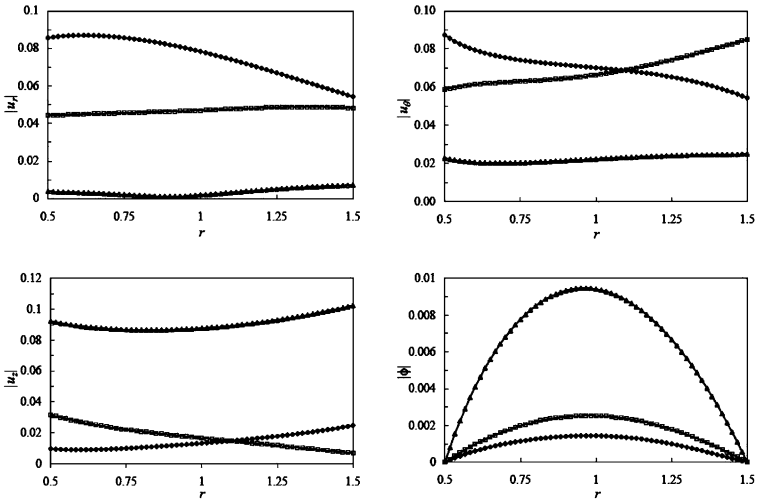

Fig. 8. Generalized displacements in a shorted–shorted cylinder along $(r, \pi/4, h/4)$ due to external loads applied at $(r_{\text{out}}, 0, 0)$ for $\omega = 1.5$ ((—□—): radial load, (—◇—): circumferential load, (—△—): axial load, (—○—): point charge).

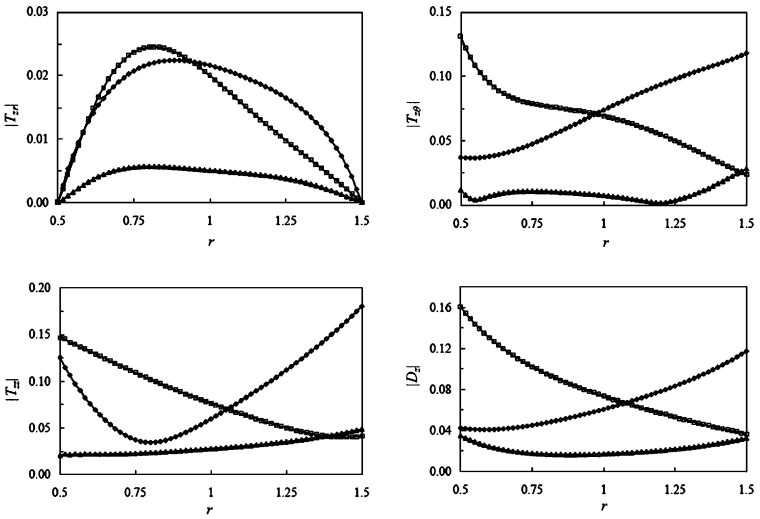

Fig. 9. Generalized stresses in a shorted–shorted cylinder along $(r, \pi/4, h/4)$ due to external loads applied at $(r_{\text{out}}, 0, 0)$ for $\omega = 1.5$ ((—□—): radial load, (—◇—): circumferential load, (—△—): axial load, (—○—): point charge).

to within an arbitrary constant for the opened–opened circuit condition, the inner surface can be grounded without loss of generality. From Figs. 6 and 8, observe that the radial and circumferential displacements dominate the response for radial and circumferential source loads, while axial displacement and electric potential manifest greater responses for the axial point load and the electric charge. This behavior is due to the nature of the PZT-4 material that evinces strong piezoelectric coupling between the axial components of stress and electric field, E_z. The shear stress T_{zr} is much smaller than the other components as seen in Figs. 7 and 9.

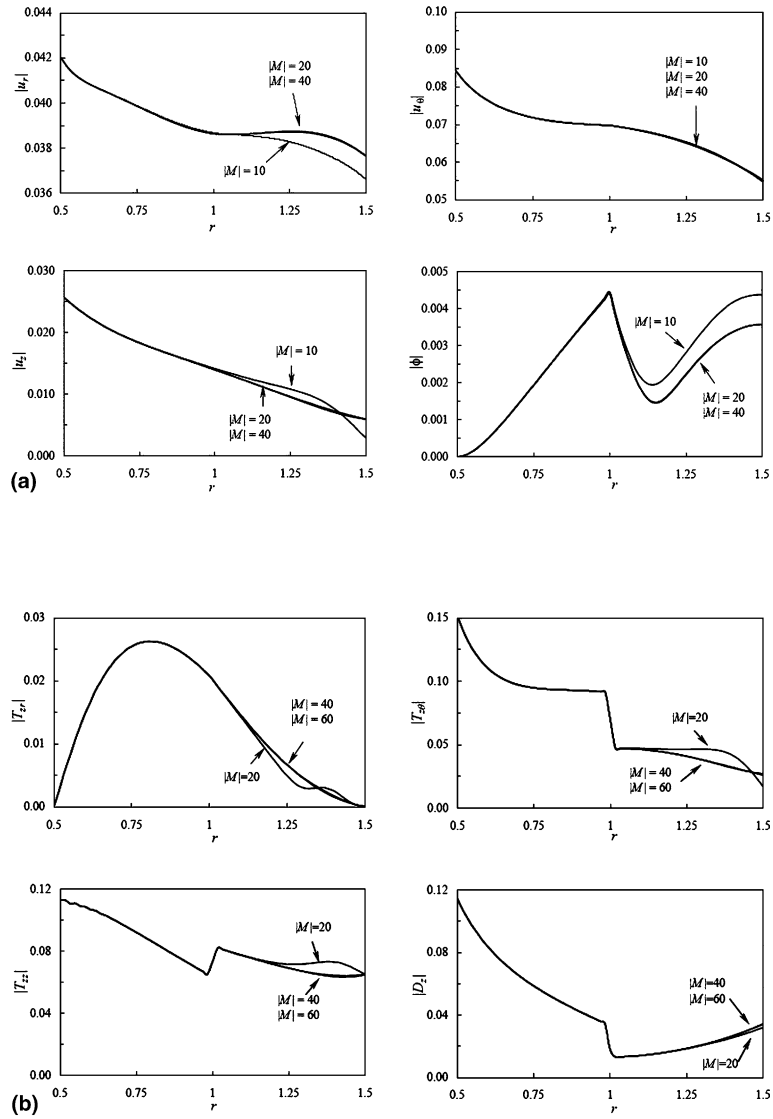

Fig. 10. (a) Generalized displacements of Green's function for a two-layer opened–opened piezoelectric cylinder due to a radial point load on the outer surface. (b) Generalized stresses of Green's function for a two-layer opened–opened piezoelectric cylinder due to a radial point load on the outer surface.

7.2. Two-layer PZT-4 cylinder

In this example, opened–opened lateral surface conditions were assumed. It was again found that for a normalized steady-state frequency of $\omega = 1.5$, 30 elements were deemed to be sufficient for good precision of the near-field quantities. The convergence characteristics are shown in Fig. 10(a and b) for a unit radial load on the outer surface. Convergence was obtained with essentially the same number of circumferential modes as the homogeneous PZT-4 cylinder. Profile plots of the displacement, stress, electric displacement and potential at the near field location of $(\theta, z) = (\pi/4, h/4)$ are shown in Figs. 11 and 12 for the set of point loads and point charge.

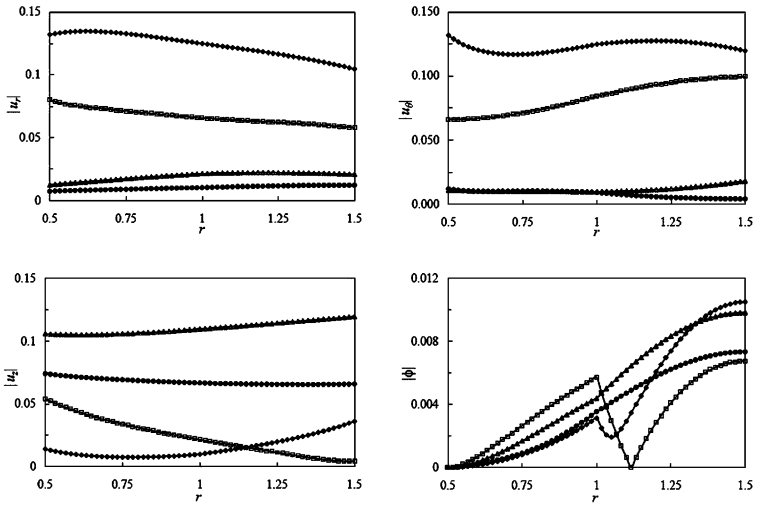

Fig. 11. Generalized displacements for a two-layered piezoelectric cylinder due to a point load ((—□—): radial load, (—◇—): circumferential load, (—△—): axial load, (—○—): point charge).

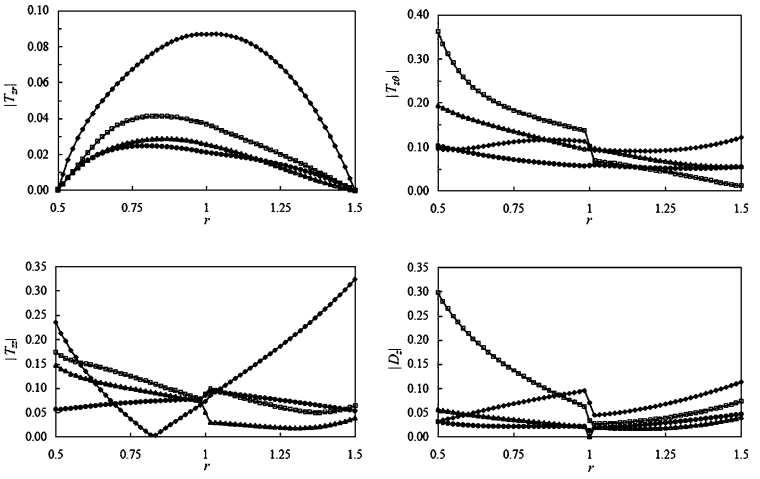

Fig. 12. Generalized stresses for a two-layered piezoelectric cylinder due to a point load ((—□—): radial load, (—◇—): circumferential load, (—△—): axial load, (—○—): point charge).

8. Conclusions

Steady-state Green functions for a laminated piezoelectric cylinder were constructed where the circumferential behavior was represented by Fourier series and the axial dependence treated by a Fourier transform. Their implementation is based on modal data from the spectral decomposition of the differential operator of the governing equation. Our Green's functions are essentially by a double summation of these data. The convergence and precision of this double summation was discussed for the two cylinders, considering both opened–opened and shorted–shorted electric surface conditions. The study of the convergence characteristics revealed the necessary number of elements in the radial discretization as well as the required number of circumferential modes for an acceptable precision of the Green's functions depicting the four different source terms, i.e., mechanical loads and electric charge. The required number of modes in their representations was quite nominal and was far from being exorbitantly large. Thus, Green's functions in these forms should be useful in other applications.

References

Berlincourt, D.A., Curran, D.R., Jaffe, H., 1964. Piezoelectric and piezomagnetic materials and their function in transducers. Physical Acoustics 1 (Part A), 169–270.

Buchanan, G.R., Peddieson Jr., J., 1989. Axisymmetric vibration of infinite piezoelectric cylinders using one-dimensional finite elements. IEEE Transactions on Ultrasonics, Ferroelectrics and Frequency Control 36 (4), 459–465.

Buchanan, G.R., Peddieson Jr., J., 1991. Vibration of infinite piezoelectric cylinders with anisotropic properties using cylindrical finite element. IEEE Transactions on Ultrasonics, Ferroelectrics and Frequency Control 38 (3), 291–296.

Chen, W.Q., Bian, Z.G., Lv, C.F., Ding, H.J., 2004. 3D free vibration analysis of a functionally graded piezoelectric hollow cylinder filled with compressible fluid. International Journal of Solids and Structures 41 (3–4), 947–964.

Ding, H.J., Chen, W.Q., Guo, Y.M., Yang, Q.D., 1997. Free vibrations of piezoelectric cylindrical shells filled with compressible fluid. International Journal of Solids and Structures 34 (16), 2025–2034.

Ding, H.J., Wang, H.M., Hou, P.F., 2003. The transient response of piezoelectric hollow cylinders for axisymmetric plane strain problems. International Journal of Solids and Structures 40, 105–123.

Dökmeci, M.C., 1980. Recent advances/vibrations of piezoelectric crystals. International Journal of Engineering Science 18, 431–448.

Dökmeci, M.C., 1989. Recent advances in the dynamic applications of piezoelectric crystals. The Shock and Vibration Digest 21, 3–20.

Hussein, M.M., Heyliger, P.R., 1998. Three-dimensional vibrations of layered piezoelectric cylinders. Journal of Engineering Mechanics 124 (11), 1294–1298.

Paul, H.S., 1962. Torsion vibrations of circular cylindrical shells of piezoelectric crystals. Archiwum Mechaniki Stosowanej 1, 123–133.

Paul, H.S., 1966. Vibrations of circular cylindrical shells of piezoelectric silver iodide crystals. Journal of the Acoustical Society of America 40 (5), 1077–1080.

Paul, H.S., Raju, D.P., 1981. Asymptotic analysis of the torsional modes of wave propagation in a piezoelectric solid cylinder of (622) class. International Journal of Engineering Science 19 (8), 1069–1076.

Paul, H.S., Raju, D.P., 1982. Asymptotic analysis of the modes of wave propagation in a piezoelectric solid cylinder. Journal of the Acoustical Society of America 71 (3), 255–263.

Paul, H.S., Venkatesan, M., 1987. Vibrations of a hollow circular cylinder of piezoelectric ceramics. Journal of the Acoustical Society of America 82 (3), 952–956.

Siao, J.C.-T., Dong, S.B., Song, J., 1994. Frequency spectra of laminated piezoelectric cylinders. ASME Journal of Vibration and Acoustics 116, 364–370.

Tiersten, H.F., 1969. Linear Piezoelectric Plates. Plenum Press, New York.

Zhu, J., Shah, A.H., Datta, S.K., 1995. Modal representation of two-dimensional elastodynamic Green's functions. ASCE Journal of Engineering Mechanics 121 (1), 26–36.

Zhuang, W., Shah, A.H., Dong, S.B., 1999. Elastodynamic Green's function for laminated anisotropic circular cylinders. ASME Journal of Applied Mechanics 66, 665–673.